J. Fluid Mech. (1993), *vol.* 256, *pp.* 535–560

Azimuthal instability of divergent flows

By VLADIMIR SHTERN AND FAZLE HUSSAIN
Department of Mechanical Engineering, University of Houston, Houston, TX 77204-4792, USA

(Received 22 April 1992 and in revised form 14 April 1993)

We investigate a new mechanism for instability (named *divergent instability*), characterized by the formation of azimuthal cells, and find it to be a generic feature of three-dimensional steady axisymmetric flows of viscous incompressible fluid with radially diverging streamlines near a planar or conical surface. Four such flows are considered here: (i) Squire–Wang flow in a half-space driven by surface stresses; (ii) recirculation of fluid inside a conical meniscus; (iii) two-cell regime of free convection above a rigid cone; and (iv) Marangoni convection in a half-space induced by a point source of heat (or surfactant) placed at the liquid surface. For all these cases, bifurcation of the secondary steady solutions occurs: for each azimuthal wavenumber $m = 2, 3, \ldots$, a critical Reynolds number (Re_*) exists. The intent to compare with experiments led us to investigate case (iv) in more detail. The results show a non-trivial influence of the Prandtl number (Pr): instability does not occur in the range $0.05 < Pr < 1$; however, outside this range, $Re_*(m)$ exists and has bounded limits as Pr tends to either zero or infinity. A nonlinear analysis shows that the primary bifurcations are supercritical and produce new stable regimes. We find that the neutral curves intersect and subcritical secondary bifurcation takes place; these suggest the presence of complex unsteady dynamics in some ranges of Re and Pr. These features agree with the experimental data of Pshenichnikov & Yatsenko ($Pr = 10^3$).

1. Introduction

In this paper, we investigate a new instability mechanism for three-dimensional steady flows of viscous incompressible fluid with radially divergent streamlines near a planar or conical surface. Bifurcations of initially axisymmetric flows lead to the appearance of secondary steady solutions of the Navier–Stokes equations; the corresponding flow patterns display the presence of azimuthal cells. The first indication of such an instability mechanism was found in the planar source flow (Goldshtik, Hussain & Shtern 1991). This source flow does not possess well-known conditions for instability such as a jump or an inflexion point in the velocity profile, or unstable stratification of swirl; hence, this is definitely not a case of the Helmholtz, Rayleigh or Taylor instability. We call this *divergent instability*. This instability, inertial in nature, is a kind of inner separation caused by an unfavourable pressure gradient. The flow tends to move away from the regions of increased pressure, resulting in the splitting of the initially azimuthally uniform flow into a few separated radial jets. The present study explores if this instability is generic and strong enough to occur in non-planar flows where the divergence takes place only in a part of the flow region and boundary conditions can provide the stabilizing influence.

As examples of such flows, we have chosen the conically similar jet-like flows (see Goldshtik & Shtern 1990*a*). In particular, we study: (i) the Squire–Wang solution (Squire 1952; Wang 1971, 1991) which models the oceanic motion induced by a tanker

crash (figure 1*a*); (ii) generalization of the previous solution for conical regions with a free surface (figure 1*b*) which models recirculation of a liquid in the conical meniscus of an electrified needle used for electrosprays (Hayati, Bayley & Tadros 1986; Bayley 1988); (iii) a two-cell flow above rigid cones (figure 1*c*) which models free convection near a glacier (Goldshtik & Shtern 1990*b*); and (iv) Marangoni convection in a half-space induced by a point source of heat or surfactant placed on the surface of a liquid (figure 1*d*).

Three reasons are behind such a choice of flows. First, the divergent instability is expected to occur in these flows as the streamlines diverge radially near a planar or a conical surface. Second, these flows are exact analytical solutions of the equations considered (the solution of Bratukhin & Maurin 1967 is the only known analytical solution of the Navier–Stokes and heat equations for the nonlinear Marangoni problem), which simplifies the stability analysis. Third, results from an experiment on Marangoni convection (Pshenichnikov & Yatsenko 1974) seem to contradict the exact solution; our objective was to resolve this contradiction.

The governing equations and boundary conditions for the conically similar class of flows are introduced (§2), followed by a review of the analytical solutions for the basic axisymmetric flows (§3), Pshenichnikov & Yatsenko's experiment (§4) and the problem formulation for finding the neutral curves (§5). Next, an analytical and numerical study of bifurcation in flows (i)–(iv) is presented in §§6, 7.1, 7.2 and 8 respectively. The asymptotic behaviour at high Pr for the Marangoni convection is discussed in §9, where we deduce the limiting boundary conditions (§9.1), calculate the limiting Re_* (§9.2), derive the asymptotic law at large m (§9.3), and calculate the neutral curves (§9.4). A nonlinear analysis of bifurcation in the Marangoni convection (§10) reveals prominent features of the secondary regimes such as the supercritical nature of the bifurcations as well as the effects of the subharmonic resonance. Finally we discuss (§11) and list (§12) the main results.

2. Problem formulation

First, we will formulate the problem for the general case. The equations of interest are the Navier–Stokes equations,

$$\boldsymbol{v}\cdot\boldsymbol{\nabla}\boldsymbol{v} = -\frac{1}{\rho}\boldsymbol{\nabla}p + \nu\Delta\boldsymbol{v}, \quad \boldsymbol{\nabla}\cdot\boldsymbol{v} = 0, \tag{1}$$

and the heat equation,

$$\boldsymbol{v}\cdot\boldsymbol{\nabla}T = \kappa\Delta T, \tag{2}$$

for a viscous incompressible heat-conducting fluid. Equation (2) is analogous to a species diffusion equation, where temperature T and the thermal diffusivity κ are replaced by the species concentration and the mass diffusion coefficient respectively. Density ρ, kinematic viscosity ν, and κ are assumed to be constants, while surface tension σ is assumed to be a function of temperature or surfactant concentration (see Levich 1962). We use the linear approximation

$$\sigma = \sigma_\infty - \gamma(T - T_\infty), \tag{3}$$

where σ_∞ and T_∞ are values of σ and T far from the source. The surface stresses are related to the temperature gradient by

$$\tau_{nj} = -\gamma(\boldsymbol{\nabla}T)_j, \tag{4}$$

where the subscript n corresponds to the normal direction and the subscript j corresponds to any direction tangent to the liquid surface. In the experiment by Pshenichnikov & Yatsenko, the surface deflection was small (due to gravity and surface

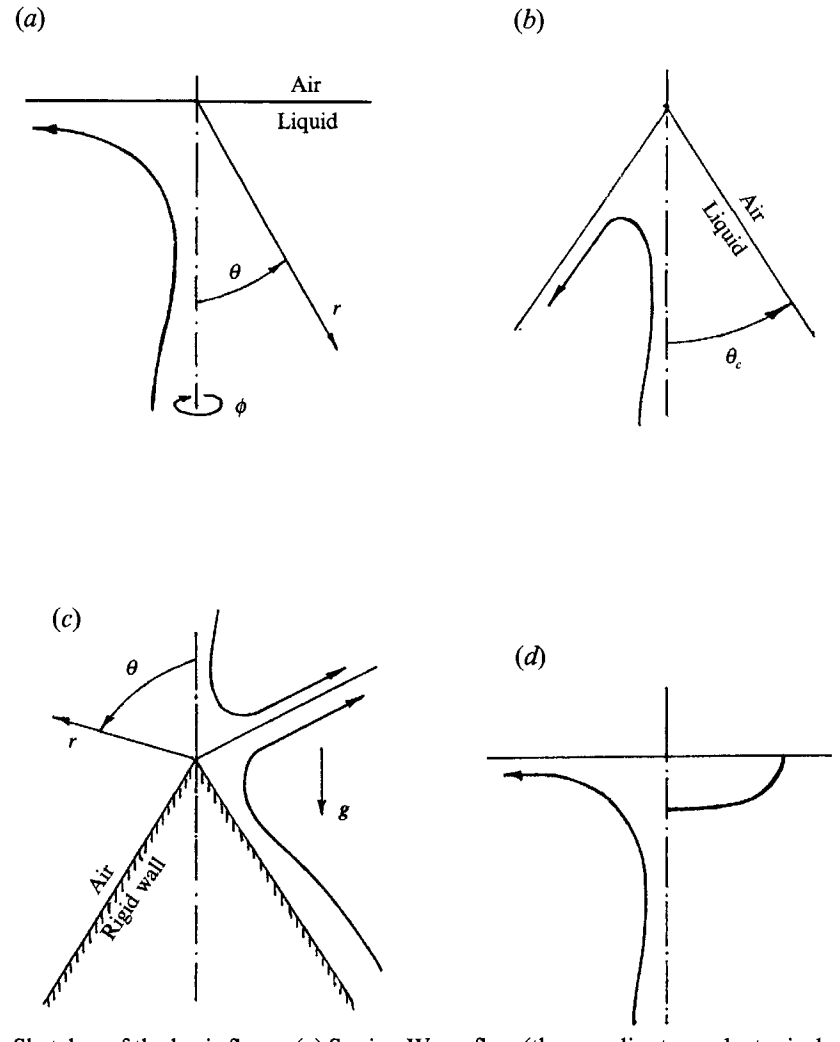

FIGURE 1. Sketches of the basic flows: (*a*) Squire–Wang flow (the coordinates and a typical streamline are shown); (*b*) flow in a conical meniscus of angle θ_c; (*c*) convection above the rigid cone, and (*d*) Marangoni problem (typical streamline (left) and isotherm (right) are shown).

tension) and there was no visible deformation of the surface; this led us to neglect deformations of the surface. Heat (mass) exchanges across the surface are also neglected in accordance with this experiment. This implies that the normal velocity and the normal projection of the temperature gradient at the surface are both zero, i.e.

$$v_n = 0, \quad \text{and} \quad (\nabla T)_n = 0. \tag{5}$$

We also assume that far from the source the fluid is at rest and $T = T_\infty$.

Equations (1)–(2) and boundary conditions (4)–(5) admit conically similar solutions, which suggest representations for velocity v, pressure p and temperature T in the following forms:

$$v_r = \frac{\nu}{r} u(\theta, \phi), \quad v_\theta = \frac{\nu}{r} \frac{y(\theta, \phi)}{\sin\theta}, \quad v_\phi = \frac{\nu}{r} \frac{\Gamma(\theta, \phi)}{\sin\theta}, \tag{6}$$

$$p = p_\infty + \rho \frac{\nu^2}{r^2} \frac{g(\theta, \phi)}{\sin^2\theta}, \quad \text{and} \quad T = T_\infty + \frac{c}{r} \vartheta(\theta, \phi), \tag{7}$$

where (r, θ, ϕ) are the spherical coordinates; r is the distance from the origin where the source of heat is placed; θ is the polar angle between the radius vector and the surface normal – we will use

$$x = \cos\theta$$

instead of θ to simplify the analysis; ϕ is the azimuthal angle around the normal direction (figure 1*a*); c is a scaling constant; and u, y, Γ, g, and ϑ are the dimensionless functions. Note, there are no intrinsic velocity and length scales in the conical flows; thus introduction of ν/r as a velocity scale is useful for comparing the results of the various problems considered here. Substitution of (6)–(7) in (1)–(2) shows that all terms are proportional to r^{-3} and yields

$$(1-x^2)\,u_{xx} = (2x-y)\,u_x - (u+2)\,u + 2F + \frac{\Gamma u_\phi - u_{\phi\phi}}{1-x^2}, \tag{8a}$$

$$(1-x^2)\,\Gamma_{xx} = -u_\phi - F_\phi - y\Gamma_x - \frac{(2x+y)\,y_\phi + \Gamma_{\phi\phi}}{1-x^2}, \tag{8b}$$

$$(1-x^2)\,\vartheta_{xx} = 2x\vartheta_x - Pr\,(y\vartheta_x + u\vartheta) - \frac{\vartheta_{\phi\phi} - Pr\,\Gamma\vartheta_\phi}{1-x^2}, \tag{8c}$$

$$(1-x^2)\,F_x = \Gamma_{x\phi} - \Gamma\Gamma_x - \frac{\Gamma y_\phi - y_{\phi\phi}}{1-x^2}, \tag{8d}$$

$$y_x = u + \frac{\Gamma_\phi}{1-x^2}, \quad \text{and} \quad F = u - \frac{2g + y^2 + \Gamma^2}{2(1-x^2)}, \tag{8e,f}$$

where the subscripts denote differentiation with respect to the corresponding variables; the auxiliary function F is introduced instead of g to simplify the analytical as well as numerical study; and $Pr = \nu/\kappa$ is the Prandtl number. Note that formulation (8) reduces the number of independent variables from three to two.

At the surface $x = 0$, boundary conditions (4) and (5) are transformed to

$$y = 0, \quad \vartheta_x = 0, \quad u_x = -Mr\,\vartheta, \quad \text{and} \quad \Gamma_x = Mr\,\vartheta_\phi, \tag{9a, d}$$

where $Mr = \gamma c/(\rho\nu^2)$ is the Marangoni number. In the purely hydrodynamic problems, since u_x is non-zero for the basic flows, the boundary conditions for disturbances assume no stress at the surface; hereafter they are referred to as *stress-free* boundary conditions.

For conical regions (9*a–d*) are applied on the cone surface $x = x_c$.

For the problem with a point source of heat, a total heat flux q is given by

$$q = kr^2 \int_0^{2\pi} \mathrm{d}\phi \int_0^{\pi/2} \left(\frac{v_r T}{\kappa} - \frac{\partial T}{\partial r}\right) \mathrm{d}\theta = 2\pi k c q_d; \tag{10}$$

where

$$q_d = \int_2^1 (\langle\vartheta\rangle + Pr\,\langle u\vartheta\rangle)\,\mathrm{d}x,$$

k is the thermal conductivity, and angle brackets denote averaging with respect to the azimuthal angle ϕ; e.g. $\langle\vartheta\rangle = (1/2\pi)\int_0^{2\pi}\vartheta\,\mathrm{d}\phi$. The value of q is assumed to be given. If ϑ is normalized so that $q_d = 1$, then $Mr = \gamma q/(2\pi k\rho\nu^2)$. In numerical computations, q_d is first evaluated by assuming $\langle\vartheta\rangle = 1$ at $x = 0$; then the normalization $q_d = 1$ is achieved through dividing ϑ by q_d.

A solution of (8)–(9) must be periodic with respect to ϕ (having a period of 2π) and

regular on the axis $x = 1$. This requirement of regularity, though physically obvious, is mathematically non-trivial as the coefficients of (8) have singularities at $x = 1$. In particular, the regularity implies

$$y = \Gamma = 0, \quad \text{and } u \text{ and } \vartheta \text{ bounded at } x = 1. \tag{11}$$

Requirements (9) and (11) provide eight boundary conditions necessary to solve (8).

3. Axisymmetric solutions

We will study stability and bifurcation of axisymmetric flows; the solutions arrived at are cited later as *basic* solutions. For a flow independent of ϕ, it follows from (8)–(11) that $\Gamma \equiv 0$, $F \equiv$ const, and $y_x = u$; hence, (8*a*) becomes uncoupled and can be integrated analytically (Squire 1952). The solution is

$$y = 2\lambda(1-x)\frac{1-[(1+x)/(1+x_c)]^\gamma}{\lambda/\mu-[(1+x)/(1+x_c)]^\gamma}, \quad x_c \leqslant x \leqslant 1, \tag{12}$$

$$\lambda = \tfrac{1}{2}(1+\gamma), \quad \mu = \tfrac{1}{2}(1-\gamma), \quad \gamma = (2Re+1)^{\frac{1}{2}},$$

where $Re = r\langle v_r\rangle_c/\nu$ is the Reynolds number, and the subscript c denotes a value of the radial velocity at the cone boundary $x = x_c$ (for the planar boundary, $x_c = 0$). Introduction of this particular form of Re is convenient for comparison of the stability of the various flows considered here. The divergent motion near the boundary corresponds to $Re > 0$ and the convergent motion corresponds to $Re < 0$. Most of our results are for $Re > 0$.

The axisymmetric case (8*c*) also has the analytical solution (Bratukhin & Maurin 1967):

$$\vartheta = \vartheta_0[(\lambda/\gamma)(1+x)^\mu - (\mu/\gamma)(1+x)^\lambda]^{-2Pr}. \tag{13}$$

The surface temperature ϑ_0 is defined by the condition $q_d = 1$.

Differentiating (12) and using $x_c = x = 0$, we have $u_x(0) = -2Re$. Then from (9*c*) we obtain $Mr\,\vartheta_0 = 2Re$. For $Pr = 0$, when $\vartheta \equiv \vartheta_0 = 1$, this becomes

$$Mr = 2Re. \tag{14}$$

In the limiting case, $Pr \to \infty$, ϑ tends to zero everywhere except possibly at $x = 0$. Near $x = 0$, the approximation $y = xRe$ together with (13) and the condition $q_d = 1$ yields

$$\vartheta = \vartheta_0 \exp(-\tfrac{1}{2}Pex^2), \quad \text{and} \quad \vartheta_0 = \left(\frac{2}{\pi Pe}\right)^{\frac{1}{2}}; \tag{15}$$

where $Pe = Pr\,Re$ is the Péclet number. Therefore, for $Pr \gg 1$ we have

$$Mr^2 = 2\pi Pr\,Re^3. \tag{16}$$

The relations (14), (16) are essential to compare our results with those of Bratukhin & Maurin (who have used $A = 2Re$), with those of Wang (who used $B/\nu = Re$), and with experimental data by Pshenichnikov & Yatsenko (who used $Q = 2\pi Mr$).

4. Prior experimental evidence

A major motivation for the Pshenichnikov & Yatsenko experiment was to provide a direct comparison with the theoretical solution by Bratukhin & Maurin (1967); however, they observed a different flow pattern than that predicted by the theoretical

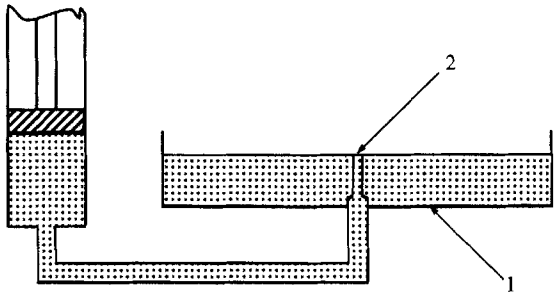

FIGURE 2. Set-up of the Pshenichnikov & Yatsenko experiment for Marangoni convection. A 10% alcohol–water solution flows in through tube (2) in the cylindrical pan (1) filled with distilled water.

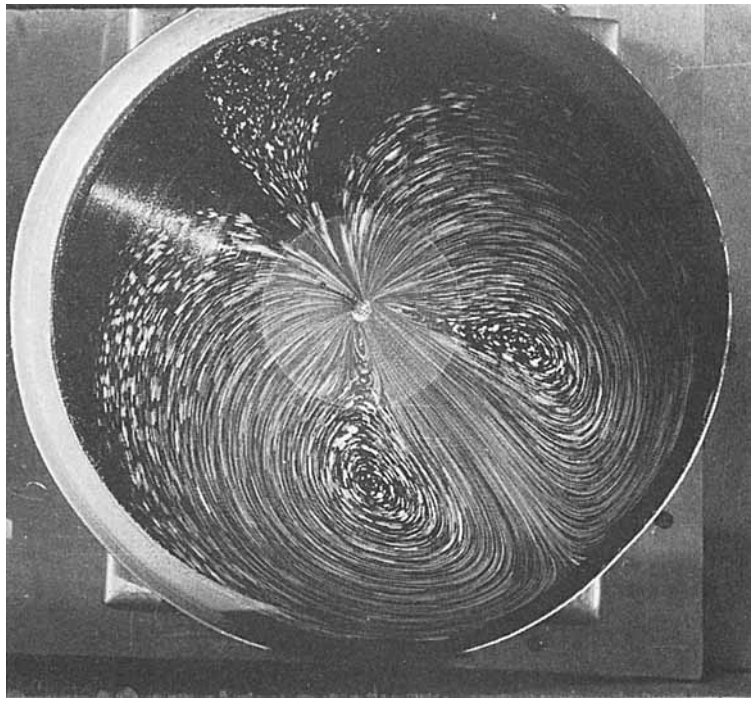

FIGURE 3. Two-cell regime of the Marangoni convection (top view).

solution. Since Pshenichnikov & Yatsenko's results are closely related to our analysis, and taking into account that their publication is not easily accessible, a brief review of their experimental results seems necessary. Figure 2 shows a schematic of the set-up. Distilled water fills the cylindrical pan (1) of 280 mm diameter and 40 mm height. A 10% alcohol–water solution flows in through the thin capillary tube (2) at an extremely slow flow rate (from 0.0003 to 0.1 g/s). Even though heating is due to dissolution, the thermocapillary effect is 500 times weaker than the surfactant action and can be neglected. Aluminium powder and time-lapse photography were used to visualize flow patterns. At low flow rates, a two-vortex regime exists (figure 3, top view). The number of vortices becomes 4, 6, 8 (figure 4) and 10, as the flow rate is increased gradually. As the flow rate decreases, the number of vortices also decreases; however, critical flow rates (corresponding to transitions between the regimes) are less than those when the

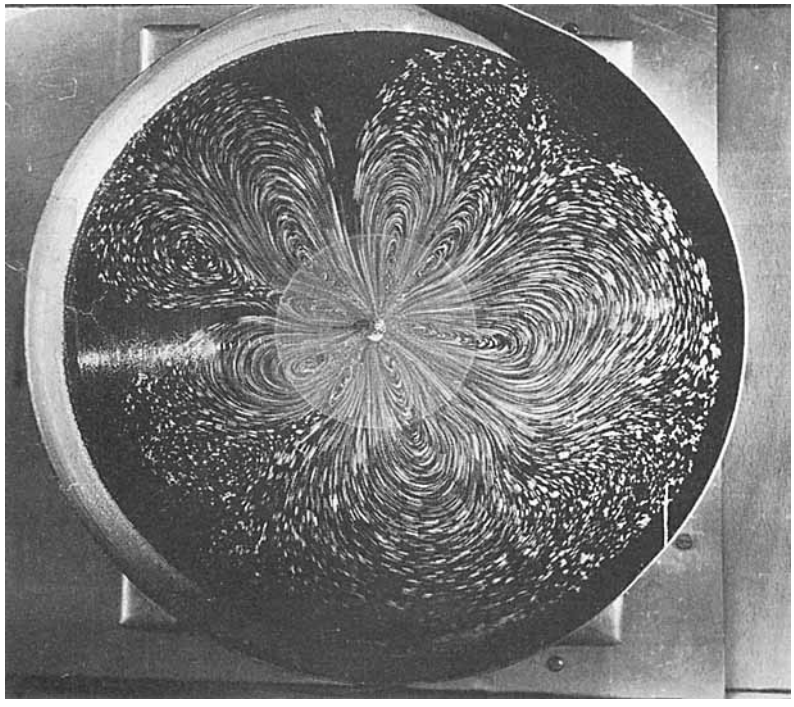

FIGURE 4. Eight-cell regime (top view).

flow rate increases. For instance, the four-cell regime appears at $Q_+ = 2.7 \times 10^6$, but disappears (when the flow rate decreases) at $Q_- = 1.9 \times 10^6$. The Schmidt number is 10^3, so the Re, calculated with the help of (16), are $Re_+ = 310$ and $Re_- = 240$. Thus, the transitions between regimes with different cell numbers have a hysteretic nature. When the flow rate increases, unsteady regimes are observable in some ranges of Q near its critical value, where the cell number alternates randomly in time.

5. Linear analysis

To study stability, it is necessary to consider how the disturbances develop in time and space. Since, in general, the disturbances are not self-similar, this problem is rather complex for conical flows. In addition, the existence of a singularity at $r = 0$ in the class (6)–(7), together with the fact that a general theory of stability and bifurcation for singular solutions has not yet been developed, enhances the complexity of the situation. However, bifurcations of the new solutions of the reduced system (8) can be studied rather easily by well-known procedures. Here we solve this bifurcation problem, and then discuss the stability of the solutions, assuming that the connection between stability and bifurcation is the same as for non-singular solutions.

The difference between two steady solutions may be considered as a neutral disturbance. This disturbance becomes infinitesimal at the bifurcation point $Re = Re_*$. The corresponding spectral problem of the linear stability theory (where disturbances have a factor $\exp(\lambda t)$, λ being a real number) has a solution with $\lambda = 0$ at $Re = Re_*$. Function $\lambda(Re)$ either changes its sign at $Re = Re_*$ (signifying instability) or merely touches the abscissa. The latter case is not robust and, hence, not expected at arbitrary values of other parameters such as Pr and x_c.

A detailed investigation of the connection between stability and bifurcation characteristics already exists for planar flows (Goldshtik *et al.* 1991). This investigation shows that the spatially and temporally developing disturbances are not self-similar and have different singularities; nevertheless they undergo transitions between the primary and secondary self-similar solutions. The same is expected to occur in the three-dimensional case considered here; thus, this study will be confined to that of neutral disturbances and established secondary regimes only.

The necessary condition for bifurcation is the existence of a non-trivial solution of (8) linearized near the basic solution. The basic solutions (12) and (13) do not depend on ϕ; hence the linearized equations have 'normal mode' solutions for disturbances, which are the Fourier harmonics with respect to ϕ with period 2π. Taking into account an arbitrary phase shift, we look for a solution in the following form:

$$\begin{gathered} u = u_b(x) + u_1(x)\cos(m\phi), \quad y = y_b(x) + y_1(x)\cos(m\phi), \\ F = F_b(x) + F_1(x)\cos(m\phi), \\ \vartheta = \vartheta_b(x) + \vartheta_1(x)\cos(m\phi), \\ \text{and} \quad \Gamma = \Gamma_1(x)\sin(m\phi), \end{gathered} \tag{17}$$

where the subscripts b and 1 correspond to the basic solution and the disturbances respectively; and the representation for Γ follows from (8*e*). Substituting (17) in (8), and neglecting terms which are nonlinear with respect to the disturbances, we obtain

$$(1-x^2)u_1'' = (2x-y_b)u_1' - u_b' y_1 - 2(u_b+1)u_1 + 2F_1 + \frac{m^2 u_1}{1-x^2}, \tag{18a}$$

$$(1-x^2)\Gamma_1'' = m\frac{m\Gamma_1 + y_1(2x+y_b)}{1-x^2} + m(u_1+F_1) - y_b\Gamma_1', \tag{18b}$$

$$(1-x^2)\vartheta_1'' = 2x\vartheta_1' - Pr(y_b\vartheta_1' + u_b\vartheta_1 + \vartheta_b' y_1 + \vartheta_b u_1) + \frac{m^2\vartheta_1}{1-x^2}, \tag{18c}$$

$$(1-x^2)F_1' = m\Gamma_1' - \frac{m^2 y_1}{1-x^2}, \quad \text{and} \quad y_1' = u_1 + \frac{m\Gamma_1}{1-x^2}, \tag{18d, e}$$

where the prime denotes differentiation with respect to x. The boundary conditions at the surface are, from (9) and (17),

$$y_1 = 0, \quad \vartheta_1' = 0, \quad u_1' = -Mr\,\vartheta_1, \quad \text{and} \quad \Gamma_1' = -mMr\,\vartheta_1 \quad \text{at} \quad x = 0. \tag{19}$$

For the Squire–Wang problem, we use (19) with $Mr = 0$ and $\vartheta_1 \equiv 0$. For the flow with a conical boundary, the conditions (19) are used at $x = x_c$. The disturbances at the axis must satisfy

$$y_1 = \Gamma_1 = u_1 = \vartheta_1 = 0 \quad \text{at} \quad x = 1. \tag{20}$$

Here u_1 and ϑ_1 need to be zero to make u and ϑ single-valued at $x = 1$.

Obviously, the problem (18)–(20) has a trivial (zero) solution. To find a non-trivial solution, the following algorithm is adopted. In addition to (19), we choose $F_1(0) = 1$ (normalization) and some tentative values of $\Gamma_1(0)$, $u_1(0)$ and $\vartheta_1(0)$. We then integrate (18) as an initial-value problem from $x = 0$ to $x = x_f = 1-\epsilon$. As a rule, we choose $\epsilon = 0.001$ to avoid the singularity at $x = 1$. We have occasionally checked that decreasing ϵ further does not change the calculated parameters up to at least three digits. The next step is to select $\Gamma_1(0)$, $u_1(0)$ and $\vartheta_1(0)$ using the shooting method to satisfy the conditions $\Gamma_1(x_f) = u_1(x_f) = \vartheta_1(x_f) = 0$. This linear problem has a unique

solution. Finally, we study $y_1(x_f)$ as a function of the relevant parameters, say Re or Pr, and look for the zeros of this function that are identical with the critical values (Re_* or Pr_*).

6. Instability of the Squire–Wang flow

6.1. *Numerical results*

The calculations become simpler for a purely hydrodynamic problem – in particular, for the Squire–Wang flow (figure 1*a*). The divergent instability with respect to disturbances corresponding to $m = 1$ does not occur; however, a countable infinite set of Re_* exists corresponding to $m = 2, 3, \ldots$. The values of the first nine Re_* are

m	2	3	4	5	6	7	8	9	10
Re_*	18.92	33.83	52.43	73.5	99.7	130	164	202	244

The divergent instability does not occur in the convergent flow, i.e. for $Re < 0$. With increasing Re, the first instability occurs at $m = 2$. This disturbance mode begins to grow for $Re > 18.92$. Figure 5 shows eigenfunctions for $Re_* = 18.92$. Near the free surface, the disturbance velocity field has a four-vortex flow pattern described by

$$v_r = \frac{\nu}{r} u_1(0) \cos(2\phi), \quad v_\phi = \frac{\nu}{r} \Gamma_1(0) \sin(2\phi), \quad \text{and} \quad v_\theta = 0,$$

where, as evident from figure 5, the amplitude of oscillation in the radial velocity is larger than that in the azimuthal velocity. In the near-axis region ($\theta < 60°$), the radial velocity is very small in comparison with the meridional and azimuthal velocities, which are nearly equal. This corresponds to a four-cell motion on any spherical surface given by $r =$ constant. Note that Re_* increases with increasing m. To check if a set of Re_* is countably infinite, we now consider the limiting case, as $m \to \infty$, analytically.

6.2. *Asymptotic analysis for large m*

The wavenumber m corresponding to a disturbance which starts growing first, as Re increases or Pr changes, can be arbitrarily large (for example, see figure 8). Therefore, the case of $m \gg 1$ has not only mathematical interest but also physical importance. We expect that for large m, Re_* is also large. At large Re, a boundary layer develops near the surface. For the basic flow, Wang (1971) studied this limiting case by introducing the inner variables $\eta = x(\frac{1}{2}Re)^{\frac{1}{2}}$ and $Y = y(2Re)^{-\frac{1}{2}}$, using these variables in (11), and finally allowing Re to tend to infinity. The boundary-layer solution was found to be $Y = \tanh(\eta)$; this solution corresponds to a near-surface fan jet. The outer solution is $Y = 1 - x$; this corresponds to a potential upward flow.

We now consider the stability of this boundary-layer solution. Using the above-mentioned inner variables in (18) together with

$$Y_1 = y_1(\tfrac{1}{2}Re)^{\frac{1}{2}}, \quad G = \Gamma_1 Re/(2m), \quad \text{and} \quad M = m(\tfrac{1}{2}Re)^{-\frac{1}{2}}, \tag{21}$$

we reduce the system (18) in the limit $Re \to \infty$ to

$$u_1'' = (M^2 - 4Y')u_1 - 2Yu_1' - 2Y''Y_1, \tag{22a}$$

$$G'' = M^2 G - 2Y(G' - Y_1) + u_1 + F_1, \tag{22b}$$

$$Y_1' = u_1 + M^2 G, \quad \text{and} \quad F_1' = M^2(G' - Y_1). \tag{22c, d}$$

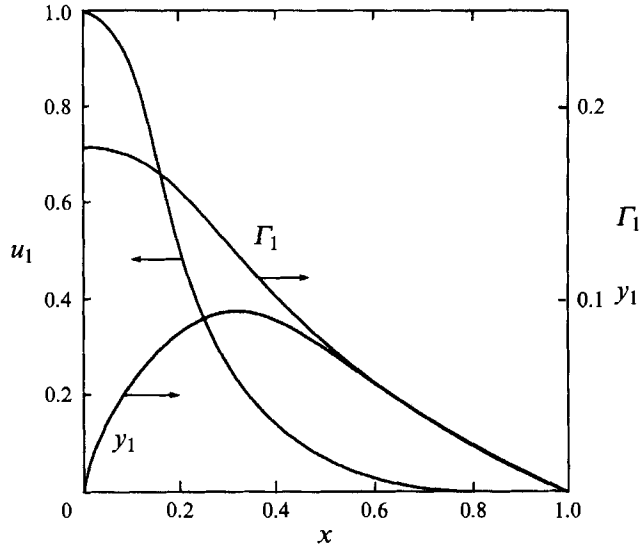

FIGURE 5. Dependence of radial (u_1), meridional (y_1) and azimuthal (Γ_1) velocities on the polar angle for neutral disturbances at $Pr = 0$, $m = 2$ and $Re = 18.92$.

Here we have taken into account that $\vartheta_1 \equiv 0$ and the prime now denotes differentiation with respect to η. It follows from (19) that

$$Y_1 = 0, \quad u_1' = 0, \quad \text{and} \quad G' = 0 \quad \text{at} \quad \eta = 0. \tag{23}$$

Moreover, Y_1, u_1 and G must decay as $\eta \to \infty$. Differentiating (22d) and substituting for G'' and Y_1' from (22b, c), one finds that F_1 must be a solution of the decoupled problem:

$$F_1'' + 2YF_1' = M^2F_1, \quad F_1'(0) = 0, \quad \text{and} \quad F_1(\infty) = 0. \tag{24a–c}$$

Here (24b) follows from (22d), and (24c) from (22b) and (23). We find that problem (24) has only the trivial solution $F_1 \equiv 0$.

Then (22d) yields $Y_1 = G'$, and (22a, c) may be rewritten as

$$u_1'' = (M^2 - 4Y')u_1 - 2Yu_1' - 2Y''G', \quad G'' = M_2G + u_1, \tag{25a, b}$$

$$u_1'(0) = G'(0) = 0, \quad \text{and} \quad u_1(\infty) = G(\infty) = 0.$$

This problem has the following analytical solution:

$$M = 1, \quad u_1 = \cosh^{-3}\eta, \quad G = -(2\cosh\eta)^{-1}, \quad \text{and} \quad Y_1 = \sinh\eta/(2\cosh^2\eta). \tag{26}$$

This can be easily verified by substituting (26) in (25). Thus, a countable infinite set of critical Re following the asymptotic law,

$$Re_* = 2m^2, \tag{27}$$

indeed exists! Our numerical calculations agree with (27) and provide the next terms of the expansion: $Re_* = 2m^2 + 61.6 - 1760m^{-2}$ – a good approximation for $m > 9$. Matching of the asymptotic analytical results with the numerical calculations provides a full description of the linear instability of the Squire–Wang flow. The existence of an infinite set of Re_* seems to be typical for the divergent instability, as it was for the Rayleigh–Bénard and the Taylor instabilities.

It can be easily inferred from (26) that the radial component of the disturbance velocity is proportional to u_1 and dominates the azimuthal and meridional components.

The last two are proportional to G and Y_1 respectively; both are multiplied by $(\frac{1}{2}Re)^{-\frac{1}{2}}$ according to (21). This implies that the instability leads to a splitting of the basic flow of a near-surface fan jet, which is azimuthally uniform, into m radial jets. This effect is quite similar to the instability of the planar source flow (Goldshtik *et al.* 1991).

7. Instability of divergent flow in cones

7.1. *One-cell motion with free boundary*

Mathematically, the problem of the stability of the fluid motion in conical domains is a slight generalization of the problem considered in the previous section. The only difference is that we consider the cone boundary ($\theta = \theta_c$), see figure 1 (*b*), to be a stress-free surface instead of a planar surface. Figure 6 shows the calculated results for the critical Re as a function of θ_c and m. It is to be noted that Re_* tends to infinity both as $\theta_c \to 0$ and $\theta_c \to \pi$. For each m, there is a specific angle θ_c, corresponding to the minimum value of Re_*. When $\theta_c \to \pi$, the basic flow approaches the case of a Landau jet propagating along the half-axis $\theta_c = \pi$, and Re_* follows the asymptotic law

$$Re_* = m(m-1)(1-x_c)/[2(1+x_c)].$$

Therefore, the Landau jet, which corresponds to $x_c = -1$, is stable with respect to these disturbance modes. The flow divergence in the core of the Landau jet corresponds asymptotically to the parabolic law: along a streamline the distance from the origin is proportional to the square of the distance from the axis. Hence, it is clear that the parabolic law of streamline divergence is not sufficient for the divergent instability to occur; for this instability one needs the linear law; i.e. streamlines must diverge asymptotically in the same manner as the rays from the origin.

When the cone angle approaches zero, the convergence decreases, and an additional stabilizing factor appears: a small gap between the axis and the cone. The physically relevant lengthscale becomes $r\sin\theta$, and asymptotically we obtain $Re_* = A/[(1-\cos\theta_c)\sin\theta_c]$, where the factor A depends on m only.

One prominent feature of this solution, as illustrated in figure 6, is that the neutral curves (for different m as $\theta_c \to 0$) intersect. At large Re, a boundary layer develops near the surface, and the maximum wavenumber m for the growing modes is proportional to $Re^{\frac{1}{2}}$ (see (27)). This implies that the azimuthal wavelength is of the same order as that of the boundary-layer thickness. Such disturbances, localized in the boundary layer, are not influenced by the damping action of the axial conditions

$$y_1 = \Gamma_1 = u_1 = 0$$

that stabilize large-scale modes of small m. This causes m_* to increase as the cone angle decreases. Such intersections are absent when $\theta_c \to \pi$, because the axis is very distant from the near-surface boundary layer and hence has little influence on the disturbances of interest. However, the viscous dissipation due to shear is larger for small-scale modes; this leads to a monotonic increase of Re_* with m.

7.2. *Two-cell motion above rigid cones*

Stress-free boundary conditions seem to be crucial for the divergent instability of near-surface flows. To study this, we chose a one-parameter family of boundary conditions which are stress-free and no-slip, respectively for the parameter value of 0 and 1. As the parameter approaches 1, Re_* tends to infinity for both the free-surface problems (i) and (ii). The next section shows that a special purely hydrodynamic problem originates from the broader problem of Marangoni convection in the limiting case of

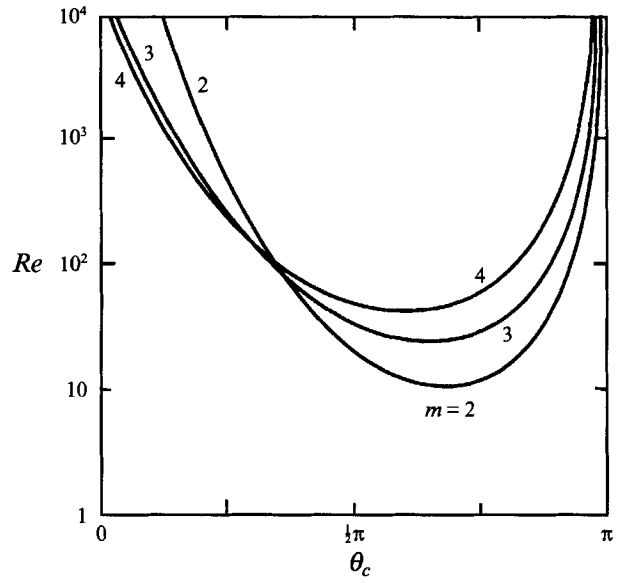

FIGURE 6. Dependence of the critical Reynolds number on cone angle θ_c and azimuthal wavenumber m for flows in the conical meniscus.

infinite Pr. There 'half-slip' boundary conditions (with zero azimuthal and non-zero radial velocities) lead to a significantly higher Re_* than that in the 'slip' case. It appears that no-slip at rigid walls effectively suppresses disturbances and prevents the instability of near-wall divergent flows. One may expect that if the divergent motion is away from the wall, the influence of no-slip boundary conditions will decrease and the divergent instability would reappear. To check this conjecture, we consider again the motion above a cone, this time subjected to the no-slip condition and driven by body forces, namely buoyancy. An appropriate example is the flow near a cone with a rigid wall. This flow models convection near a glacier. Goldshtik & Shtern (1990*b*) studied the basic flow induced by a thermal quadrupole at the cone apex. At $Pr = 0$, the heat equation decouples and the problem reduces to one of a purely hydrodynamic nature, and buoyancy serves only as an external driving force. Then the equations

$$(1-x^2)y_x+2xy-\tfrac{1}{2}y^2 = -Re[(1+x_s)/(1-x_s)](1-x)^2 f(x)/f(x_s),$$

$$f(x) = x(1+x)^2-x_c(1+x_c)^2, \quad x_s = -1-2x_c, \quad y(x_s) = 0 \quad \text{and} \quad y_x(x_s) = -Re$$

govern the basic flow. If the cone is sharp enough (i.e. its boundary $x = x_c$ satisfies the condition $x_c < -\frac{1}{3}$), then the flow has two cells (i.e. $x_c < x_s < 1$). Near the axis and wall, fluid flows to the cone apex and then forms a conical outflow (figure 1*c*); Re characterizes the radial velocity at the separating cone.

The stability problem consists of system (18), conditions (20) (with $\vartheta_1 \equiv 0$) and the no-slip conditions $y_1 = \Gamma_1 = u_1 = 0$ at $x = x_c$.

Figure 7 shows the numerical results from the solution of the above problem. It is to be noted that Re_* is of the same order as it was in the previous problems, and reaches its minimum value $Re_* = 19.3$ for the flow pattern where the outflow is near the middle cone between the conical wall $x_c = -0.6$ and the axis (see the sketch of the flow pattern for point 1 on the neutral curve). The angle ($x_{jet} = 0.36$), where the radial velocity has its maximum value, is close to the angle ($x_s = 0.33$) of the separation cone. This instability corresponds to the disturbance mode of $m = 2$.

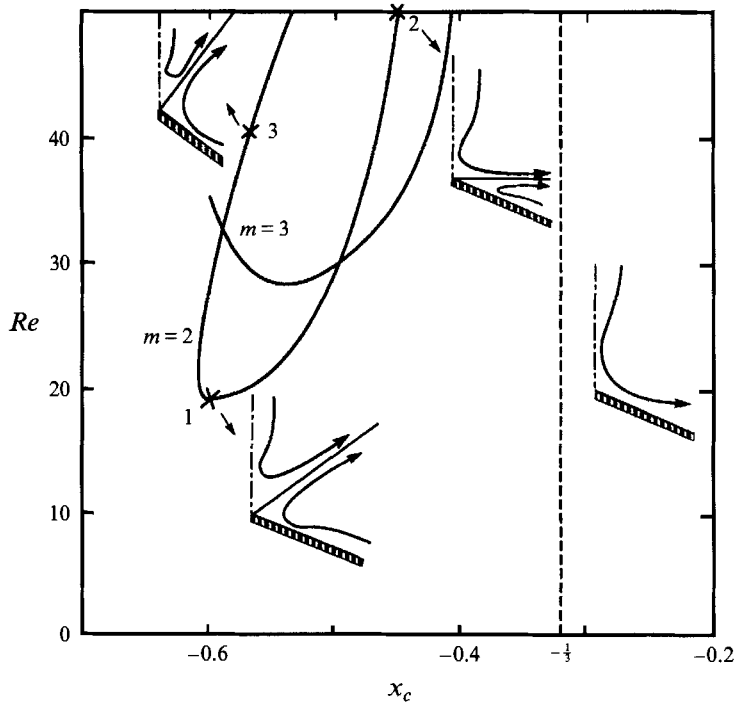

FIGURE 7. Neutral curves for flows driven by buoyancy above rigid cones. Sketches show flow patterns for points marked 1, 2 and 3 and for the one-cell regime for $x_c > -\frac{1}{3}$.

As the outflow jet approaches the wall, the stabilizing effect of the no-slip conditions is enhanced, which causes Re_* to increase along the right branch of the neutral curve. On the other hand, as the outflow jet approaches the axis, the stabilizing effect of the regularity conditions is enhanced, which causes Re_* to increase along the left branch of the neutral curve. These two cases are illustrated respectively in the flow sketches for points 2 and 3 in figure 7. The divergent instability does not occur for $x_c > -\frac{1}{3}$, when the outflow is attached to the wall. We have not found this type of instability for the one-cell upward flow either.

The divergent instability does not occur with $m = 1$ in all these cases. As m increases, the minimum Re_* also increases due to viscous dissipation. The neutral curves for different m intersect (see the arrangement of curves $m = 2$ and $m = 3$ in figure 7); the reason is the same as that in the previous case (§7.1): localization of modes with high m-values in the outflow that makes them less sensitive, in comparison with modes of small m, to the stabilizing influence of the boundary conditions.

8. Instability of Marangoni convection

8.1. *Numerical results*

Now we return to study the stability of flows with a planar free surface, namely Marangoni convection – where the hydrodynamic and thermal processes interact (figure 1 *d*). The results from numerical solutions are presented in figure 8. Two families of neutral curves, one for $Pr < 0.05$ and the other for $Pr > 1$, exist on the parametric plane (Re, Pr). At $Pr = 0$, the Marangoni problem reduces to the Squire–Wang case considered in §6. Consequently, the neutral curves, corresponding to $m = 2$, 3 and 4 at small Pr, asymptotically reach the Re_* values obtained in the Squire–Wang case

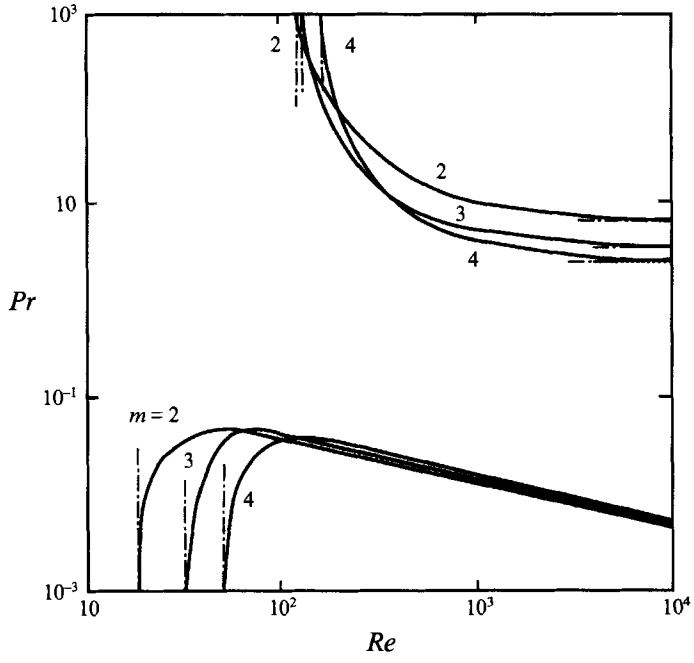

FIGURE 8. Relations between the Prandtl and Reynolds numbers for neutral disturbances for Marangoni convection. Figures near the curves denote the azimuthal wavenumber values. The dotted-dashed lines show asymptotes.

(figure 8). Pr_*, as a function of Re at a fixed m, reaches a maximum value and then decays as $Re \to \infty$. Therefore, contrary to the case of $Pr = 0$, for $Pr > 0$ each mode with $m = 2, 3, \ldots$ has a bounded instability range of Re.

Each neutral curve intersects all others; figure 8 illustrates this phenomenon for $m = 2$, 3 and 4. For large m, the intersection points can be calculated from the asymptotic analysis. We note again that the intersections provide favourable conditions for complex unsteady regimes to occur. At Re and Pr values corresponding to the intersection, a three-dimensional centre manifold exists, related to the amplitudes of the two neutral modes and to the magnitude of the azimuthal shift between the modes. This, along with existence of free parameters, $Re - Re_i$ and $Pr - Pr_i$ (where the subscript denotes the value of the corresponding parameter at the point where neutral curves intersect), makes it likely that regimes showing complex unsteady dynamics will be observed (Guckenheimer & Holmes 1983). At low Pr, the intersections take place at 'back' branches. The term 'back' branches refers to the portions of the neutral curves that lie to the right of their maxima in Pr. The complex regimes can be observed in experiment for the low-Pr range by decreasing Pr while Re remains fixed, and for the high Pr range by increasing Re while Pr remains fixed.

In our first attempt, we failed to find the family of neutral curves for large Pr by numerical methods. Presumably, this was because of the crucial role of very thin near-surface thermal boundary layers which can easily be missed during numerical calculations. Nevertheless, the asymptotic analysis described below succeeded in finding the instability expected in the high-Pr range, and observed experimentally by Pshenichnikov & Yatsenko. However, first, we will study the asymptotic features of the neutral curves at small Pr values to find the limiting relations $Pr_*(Re)$ for the back branches.

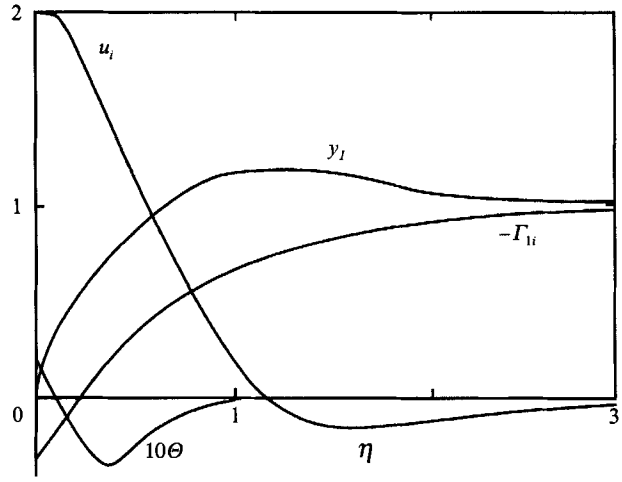

FIGURE 9. Distributions of the disturbance velocity (u_i, y_1 and Γ_{1i}) and temperature (Θ) in the boundary layer near the surface in the limit $Re \to \infty$ for $m = 2$.

8.2. *$Pr \to 0$ limit at fixed m*

To achieve this we employ the approach described in §6.2; however, here we consider m to be fixed and bounded. For the boundary layer, we again have system (22) but with $M = 0$, as dictated by (21); hence, the eigenvalue must be found in terms of a parameter different from M. Scaling analysis shows that $P = Pr(\frac{1}{2}Re)^{\frac{1}{2}}$ can serve as such a parameter. The outer solution for the basic problem, then, is

$$\left.\begin{aligned} &y_b = (2Re)^{\frac{1}{2}}(1-x), \quad u_b = -(2Re)^{\frac{1}{2}}, \quad \vartheta_b = \vartheta_0(1+x)^{-P}, \\ &\vartheta_0 = (2^{1-P}-1+P)^{-1}, \quad \text{and} \quad Mr = 2Re(2^{1-P}-1+P). \end{aligned}\right\} \tag{28}$$

The outer (external) solution for the disturbance velocity is

$$u_{1e} \equiv 0, \quad \text{and} \quad y_{1e} = -\Gamma_{1e} = [(1-x)/(1+x)]^{m/2}. \tag{29}$$

The inner solution for the disturbance velocity is

$$\left.\begin{aligned} &y_{1i} = \tanh\eta + \eta\cosh^{-2}\eta, \quad \eta = x(\tfrac{1}{2}Re)^{\frac{1}{2}}, \\ &u_{1i} = (2Re)^{\frac{1}{2}}(1-\eta\tanh\eta)\cosh^{-2}\eta, \quad \text{and} \quad \Gamma_{1i} = \tfrac{1}{3}(1-4\tanh\eta). \end{aligned}\right\} \tag{30}$$

These profiles are displayed in figure 9; the radial component of the disturbance velocity changes sign at $\eta = 1.2$, and the azimuthal component does so at $\eta = 0.25$. Thus, recirculation cells originate in a meridional section, and are placed inside the boundary layer. Outside the boundary layer, however, the amplitudes of the disturbances in radial velocity and temperature decay, and the amplitudes of the meridional and azimuthal disturbances become asymptotically equal – as predicted by relation (29).

Using the aforesaid results along with the condition (19*d*), and introducing $\Theta = \vartheta_1/Pr$, we obtain the boundary condition

$$\Theta(0) = -2[3mP(2^{1-P}-1+P)]^{-1}, \tag{31}$$

and the equation for $\Theta(x)$ which follows from (18*c*)

$$(1-x^2)\Theta'' = [2x-P(1-x)]\Theta' + \Theta\left[P+\frac{m^2}{1-x^2}\right] + \left(\frac{1-x}{1+x}\right)^{m/2} P(2^{1-P}-1+P)^{-1}(1+x)^{-1-P}. \tag{32}$$

Equation (32), along with the conditions (31) and the condition that $\Theta'(0) = 0$, defines an initial-value problem. Using the regularity condition, $\Theta(x) \sim (1-x)^{m/2}$, in the vicinity of $x = 1$, we obtain $P = 0.67$ for $m = 2$. Therefore, the asymptotic law for the neutral curve with $m = 2$ (shown in figure 8) is

$$Pr_* = 0.67(2Re)^{-\frac{1}{2}}. \tag{33}$$

The numerical results obtained are in agreement with this law.

9. Instability at Large *Pr*

9.1. *Transformation of boundary conditions*

Figure 8 shows that no linear instability occurs for $Pr > 0.05$. Our study of $y_1(x_f)$ as a function of Re and Pr (see §5) fails to find any zeros for $Pr > 0.05$. However, the case as $Pr \to \infty$, requires special treatment. This case is physically important since the Schmidt numbers (Sc), in practice, are usually very large; for example, in the Pshenichnikov & Yatsenko experiment, $Sc \approx 10^3$. (We use Pr instead of Sc throughout this paper because the thermal and concentration versions of the Marangoni problem are mathematically identical for our purpose.)

In this section we consider the transition as $Pr \to \infty$ at fixed Re and m. It was previously shown in §3 that the axisymmetric solution for ϑ has a Gaussian distribution for $Pr \gg 1$ and tends to a delta-function as $Pr \to \infty$. The physical reason is clear: at small thermal (concentration) diffusivity, the transport of heat (surfactant) is mainly convective. Because of the existence of an upward flow when $Re > 0$, all heat from the source is concentrated in a thin near-surface layer. Clearly, this is also true for a non-axisymmetric case. Integrating (8c) with respect to x in the interval $0 \leqslant x \leqslant 1$, and using (8$e$) and conditions (9) and (11), we obtain

$$\frac{\partial}{\partial \phi} \int_0^1 \frac{\vartheta_\phi - Pr\,\Gamma\vartheta}{1-x^2}\,dx = 0. \tag{34}$$

As $Pr \to \infty$, the first term in the numerator becomes negligible. Using the amplitude expansions $\Gamma = A\Gamma_1 + A^2\Gamma_2 + \ldots$, $\vartheta = \vartheta_b + A\vartheta_1 + A^2\vartheta_2 + \ldots$ and taking into account that ϑ_b tends to a delta-function due to (15), we obtain (by collecting terms of similar orders) $\Gamma_\phi = 0$ at $x = 0$. From conditions (9c, d) it follows that $u_{x\phi} + \Gamma_x = 0$. Thus, in the limit $Pr \to \infty$, (9) must be replaced by

$$y = 0, \quad u_{x\phi} + \Gamma_x = 0, \quad \Gamma_\phi = 0 \quad \text{at} \quad x = 0 \tag{35}$$

for the disturbances, and $y = \Gamma = 0$, $u = Re$ at $x = 0$ for the basic flow. In this limit, the hydrodynamic problem decouples from the thermal problem for a general non-axisymmetric nonlinear case. After solving the hydrodynamic problem, condition (9c) can be used to determine the temperature distribution at the surface for a large but finite Pr.

9.2. *Critical Reynolds numbers at* $Pr = \infty$

To solve the linear problem, we use system (18) here without (18c). Boundary conditions on the axis coincide with (20), but, instead of (19), we now apply the conditions at the surface using (17) and (35):

$$y_1 = \Gamma_1 = 0; \quad mu_1' - \Gamma_1' = 0 \quad \text{at} \quad x = 0. \tag{36}$$

Applying the algorithm described in §5.1 we get

m	2	3	4	5	6	7	8
Re_*	115	120	152	193	242	299	364

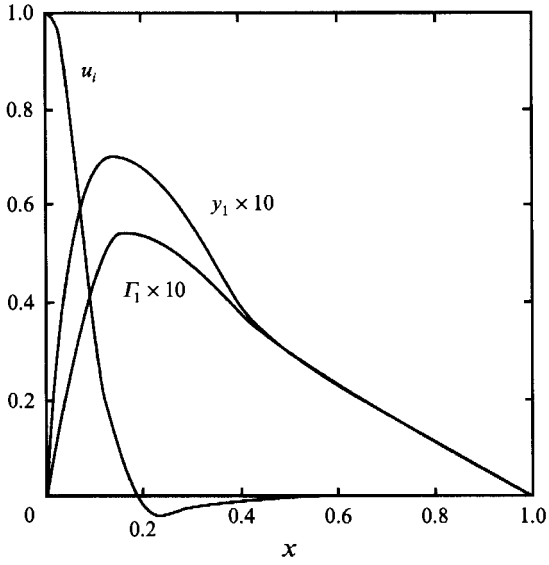

FIGURE 10. Velocity distribution for neutral disturbances at $Pr = \infty$, $m = 2$ and $Re = 115$.

These values provide the limiting Re_* for the neutral curves $Re_*(Pr)$ as $Pr \to \infty$. Figure 10 shows eigenfunctions for the first neutral mode ($Re = 115, m = 2$). At the surface, the disturbance motion is purely radial. The radial velocity predominates in the near-surface region but decreases rapidly as x increases, and is almost absent for $x > 0.5$. An infinite countable set of eigenvalues exists in this limiting case as well, and an asymptotic law for large m can be found by utilizing the same approach as in §6.2.

9.3. *Limit of large m at Pr = ∞*

We use (21) and (22) from the Squire–Wang case unchanged, but replace the boundary conditions (23) with

$$Y_1 = 0; \quad u_1' = 0; \quad G = 0 \quad \text{at} \quad \eta = 0. \tag{37}$$

No analytical solution for the problem was found; however, it can be easily solved numerically. Instead of fulfilling the decay conditions at infinity, we satisfy a set of modified conditions at a finite distance $\eta = \eta_e$. The nature of these conditions needs to be explained in more detail. The coefficients of (22*a*) become constants for $\eta \gg 1$; hence the decaying solution can be written as $u_1 = C\exp(\gamma_1 \eta)$, $\gamma_1 = -1-(1+M^2)^{\frac{1}{2}}$, which corresponds to the relation

$$u_1' - \gamma_1 u_1 = 0. \tag{38}$$

The same condition follows for F_1 from (24*a*) for $\eta \gg 1$:

$$F_1' - \gamma_1 F_1 = 0. \tag{39}$$

Equations (22*a*) and (24*a*) decouple from (22*b–d*) and admit the trivial solution $u_1 = F_1 \equiv 0$. Then from (22*d*), we have $G' - Y_1 = 0$, and (22*b*) becomes $G'' - M^2 G = 0$. It has a decaying solution given by $G = C\exp(-M\eta)$, which corresponds to the relation

$$G' + MG = 0. \tag{40}$$

Since $Y = \tanh(\eta)$ tends to 1 exponentially as $\eta \to \infty$, the value of η_e does not need to be very large to achieve sufficient accuracy. We have used $\eta_e = 6$ and have found

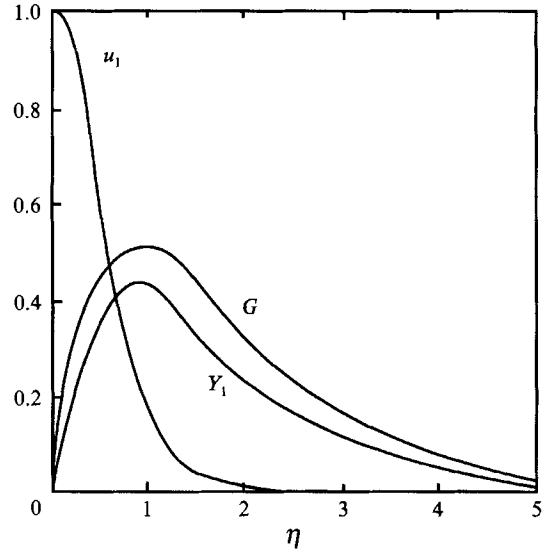

FIGURE 11. Distribution of the disturbance velocity in the boundary layer near the surface in the limit of large Re and m.

(with the help of a few tests) that increasing η_e does not result in an improved accuracy up to four decimal places. Thus, we add (37) to the normalization $u_1(0) = 1$ and the tentative values of $G'(0)$ and $F_1(0)$; then we integrate (22) as an initial-value problem from $\eta = 0$ to $\eta = \eta_e$. We find $G'(0)$ and $F_1(0)$ (by the shooting method) to satisfy (38) and (39), and finally, study the left-hand side of (40) as a function of M. The result is that this function has a unique zero at $M = 0.7624$. This corresponds to the asymptotic relation

$$Re_* = 3.44m^2 \quad \text{for} \quad m \gg 1. \tag{41}$$

Figure 11 shows distributions of the velocity components in this limit. The coefficient in (41) is larger than the coefficient in (27) and that in $Re_* = \pi(m^2-4)$, which is the law for the planar source. The reason is that the 'no-slip' condition for the azimuthal velocity, $G(0) = 0$, suppresses disturbances stronger than the 'stress-free' condition $G'(0) = 0$, which is used for the case $Pr = 0$ and for the planar source flow.

For larger Pr, the temperature in the flow differs from that in the ambient only in a thin layer near the surface. Expression (15) gives the temperature distribution for the basic solution. The disturbance relevant to temperature ϑ_1 can be expressed in the following way:

$$\vartheta_1 = (2\pi Pe)^{-\frac{1}{2}} u_1(0)\, Re^{-1}(1-\eta^2)\exp(-\tfrac{1}{2}\eta^2); \quad \eta = Pe^{\frac{1}{2}}x.$$

The function $\vartheta_1(\eta)$ changes its sign at $\eta = 1$ and satisfies the condition $\int_0^\infty \vartheta_1\, d\eta = 0$, which follows from (34) and (35).

9.4. *Neutral curves at large Pr*

Figure 8 shows, for large Pr, the numerical results for $m = 2$, 3 and 4. As $Pr \to \infty$, Re_* values approach their limits, as reported in §9.2 and shown in figure 8 by dot-dashed lines. When Re increases along the neutral curves, Pr_* monotonically decreases and tends to reach a non-zero limit as $Re \to \infty$. Consider the limiting case of large Re. In the boundary-layer approximation, the hydrodynamic part of the problem becomes

decoupled from the thermal part, and the distributions of velocity disturbances are exactly the same as those in §8.2; see (29) and (30). Unlike the case of small Pr, here there is a thermal boundary layer as well. For this layer, we again apply $\eta = x(\frac{1}{2}Re)^{\frac{1}{2}}$. For the basic solution for temperature, it follows from (13) that

$$\vartheta_b = \vartheta_0(\cosh\eta)^{-2Pr}. \tag{42}$$

We now consider temperature disturbances. In the boundary-layer limit, the first and the last terms on the right-hand side of (18*c*) become negligible in comparison with the other terms. Dropping these small terms, one can integrate (18*c*) once to obtain

$$\vartheta_1' + Pr(2/Re)^{-\frac{1}{2}}(y_b\vartheta_1 + \vartheta_b y_1) = 0,$$

where the prime denotes differentiation with respect to η. Using (42) and $y_b = (2Re)^{\frac{1}{2}}\tanh\eta$, we obtain, for the rescaled function $\Theta(\eta) = (\frac{1}{2}Re)^{\frac{1}{2}}(Pr\vartheta_0)^{-1}\vartheta_1$, the equation

$$\Theta' + 2Pr\Theta\tanh\eta = -y_1(\cosh\eta)^{-2Pr}.$$

The solution of the homogeneous equation is $\Theta = C(\cosh\eta)^{-2Pr}$, where C is the integration constant. Looking for a solution in the form $\Theta = B(\eta)(\cosh\eta)^{-2Pr}$, we then have $B' = -y_1$. Applying (30) for y_1, we obtain the solution

$$\Theta = (C - \eta\tanh\eta)(\cosh\eta)^{-2Pr}.$$

Higher-order terms of the boundary-layer expansion provide a value for the constant C, e.g. $C = \Theta(0) = 0.02$ for $m = 2$. In terms of the boundary-layer variables, (19*d*) becomes $\Gamma_1'(0) = 4m\Theta(0)$, then, applying (30) to $\Gamma_1(\eta)$, we obtain the limiting Pr_* value as $Re \to \infty$. The result is $Pr_* = 8.6$, 4.6 and 3.6 for $m = 2$, 3 and 4. As $m \to \infty$, the asymptotic Pr_* values accumulate near $Pr = 1$. For $Pr = 1$, in the boundary-layer approximation, the Reynolds analogy is relevant for temperature and velocity distributions, which yields $\Theta = \frac{1}{2}u_{1i}$ with u_{1i} given by (30).

Thus, when m increases, Re_* at $Pr = \infty$ increases and Pr_* at $Re = \infty$ decreases. Therefore, all neutral curves intersect one another. Now we proceed to study the nature of bifurcation at the neutral curves and other relevant features of nonlinear instability.

10. Nonlinear analysis

10.1. *Approach*

The objectives behind a nonlinear analysis are to examine the nature of bifurcation (whether it is subcritical or supercritical), to investigate the simplest interaction between the modes, and to inspect the features of the secondary regimes. To accomplish the above, we use the Fourier decomposition for the angle-dependent secondary steady solutions – approximated by retaining only a few modes. One may see that (8)–(10) permit solutions where functions u, ϑ, F, y are symmetric and Γ is antisymmetric with respect to ϕ. Therefore, instead of (17) we use

$$\Gamma(x,\phi) = \sum\Gamma_j(x)\sin(jm\phi), \quad j = (1,\infty), \tag{43}$$

$$u(x,\phi) = \sum u_j(x)\cos(jm\phi), \quad j = (0,\infty), \tag{44}$$

and representations similar to (44) for y, ϑ and F. The absence of the term with $j = 0$ in (43) corresponds to the fact that a mean circulation is not generated as a result of instability. In our calculations all terms with $j > 2$ are neglected. This cut-off is sufficient to portray the nature of the bifurcation and allows for estimation of the accuracy of the approximation.

Canonical approaches to the study of the bifurcation nature are weakly nonlinear and based on either the Lyapunov–Schmidt method (Yudovich 1965) or a power expansion with respect to disturbance amplitude A (Joseph 1976). They require calculations of the second harmonic and nonlinear contribution to the zeroth harmonic in $O(A^2)$. Our approach provides these quantities and therefore yields the same coefficient Re_2 as in the decomposition

$$Re = Re_* + Re_2 A^2 + \ldots$$

resulting from the canonical approaches. When the basic flow is stable for $Re < Re_*$, a subcritical or supercritical bifurcation occurs if $Re_2 < 0$ or $Re_2 > 0$ respectively. Our approach allows us to obtain good approximations of the secondary solutions in a wider range of parameters than do the canonical approaches. To estimate the intensity of a disturbance and the accuracy of the approach, we use ratios of kinetic energies of the harmonics. The total kinetic energy of the flow E is the sum of the harmonic energies: $E = E_0 + E_1 + E_2$. We use $I = [(E_1 + E_2)/E_0]^{\frac{1}{2}}$ as a measure of the disturbance intensity and $I_2 = (E_2/E_1)^{\frac{1}{2}}$ as a measure of the cut-off error. If $I_2 \ll 1$, then the approximation is satisfactory; however, if I_2 approaches 1, then higher harmonics must be taken into account.

To obtain the ODE system, we use the cut-off of (43)–(44) up to $j = 2$, substitute in (8)–(10), and make projections on the harmonics with $j = 0$, 1, and 2. This rather bulky system of the 22nd-order is given in the Appendix. It consists of eight equations for each harmonic of $j = 1$ and 2, and six equations for the zeroth harmonic. The smaller number for the zeroth harmonic is due to the absence of an equation for the circulation. The boundary conditions for the zeroth harmonic are the same as those for the basic solution, the conditions for the first harmonic coincide with (19)–(20), and the boundary conditions for the second harmonic are similar to (19)–(20).

We use a numerical algorithm similar to that used for the linear case. The results of the linear problem serve as initial values for the tentative data to start the shooting procedure, and then iterations follow until convergence. The convergence requires small steps in free-parameter variations, which seems to be a limitation of the method. On the other hand, the method provides detailed information about the dependence of the solutions on free parameters; such information sometimes helps to find the non-trivial features of the problem.

10.2. *Bifurcation character*

Our calculations show that a typical divergent instability is supercritical for the flows considered. Figure 12 shows the results for $Pr = 0$, i.e. for the Squire–Wang flow. Solid curves correspond to secondary steady axisymmetric solutions which originate at the bifurcation points, $Re = Re_*$, and exist for $Re > Re_*$. According to the general theory (Joseph 1976), such a solution is stable. Indeed, for $Re < Re_*$, the basic solution is stable and therefore attracts nearby trajectories. This implies that any disturbance with a finite (but sufficiently small) amplitude decays during some unsteady transition process. When Re is close to Re_*, an eigenplane in the phase space appears (corresponding to the neutral mode at $Re = Re_*$ with arbitrary phase shift); along that eigenplane, attraction toward the basic solution becomes weaker. For $Re > Re_*$, the basic solution repels trajectories; as a result, a circle of new steady solutions (a shift with respect to the azimuthal angle serves as the parameter) appears replacing the attractor. Figure 12 shows a typical case of evolution schematically by arrows. If the disturbance energy is smaller than that of the secondary solution, such a disturbance grows, and the transition solution tends to the secondary solution. If the disturbance

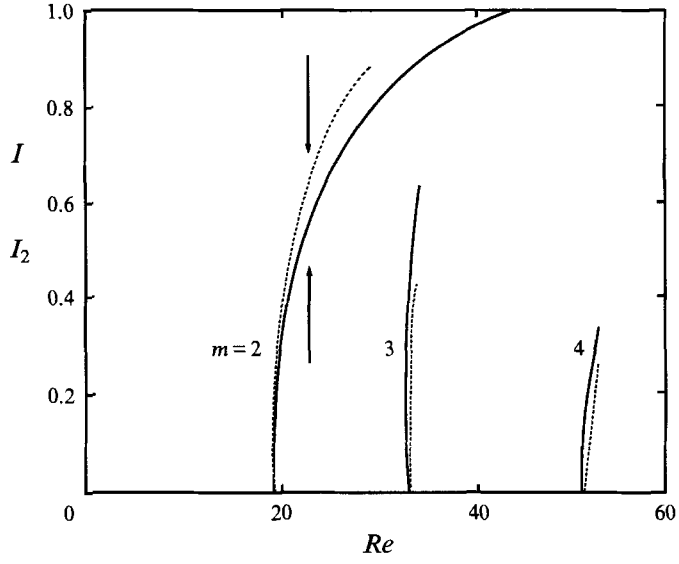

FIGURE 12. Intensity of disturbances I (—) and ratio I_2 of the second/first harmonic amplitude (·····) for the secondary steady solutions at $Pr = 0$.

energy is larger, the disturbance decays; nevertheless again the transition solution tends to the secondary solution. The solid curves in figure 12 are prone to intersect one another when disturbance energy is sufficiently large; we do not show these intersections because our calculations stop when I_2 becomes rather large (shown by the dashed lines in figure 12).

10.3. *Subharmonic resonance*

The supercritical character of the bifurcation is preserved for non-zero Pr. Figure 13 shows the neutral curves 2 and 4 (i.e. for $m = 2$ and $m = 4$) as the solid lines. The dashed lines 2′ and 2″ correspond to the secondary solutions of a small fixed amplitude for $m = 2$. Curve 2′ is below curve 2 in the (Re, Pr)-plane; this indicates that the instability is supercritical. However curve 2″ is above curve 2; this indicates that the instability is subcritical. An interesting feature is that both 2′ and 2″ cease to follow curve 2 near the intersection points of 2 and 4, i.e. at $Re \approx 100$. As 2′ and 2″ turn away from curve 2, although I is fixed, I_2 begins to increase rapidly. This indicates that the second harmonic ($j = 2$) begins to dominate the first harmonic ($j = 1$). Since the total disturbance energy is kept small, curves 2′ and 2″ approach the neutral curve 4. The secondary solutions, bifurcating along curve 4, consist of harmonics with $m = 0, 4, 8, \ldots$. That 2′ and 2″ are present near 4 indicates that a subharmonic instability occurs. This instability occurs for small I values and leads to the generation of tertiary solutions via the secondary bifurcation. The amplitude threshold for the subharmonic instability becomes zero at the intersection of curves 2 and 4. At that point, no steady secondary solution occurs corresponding to $m = 2$. Near this point complex unsteady behaviour is possible, because amplitudes of harmonics with $m = 2$ and $m = 4$, together with a phase shift between the harmonics, provide a three-dimensional dynamical system in the centre manifold. It is difficult to study this unsteady behaviour because the self-similarity is not guaranteed for time-dependent solutions. For this reason, we have restricted ourselves only to steady solutions.

Similar behaviour of neutral curves and curves for a small fixed amplitude is

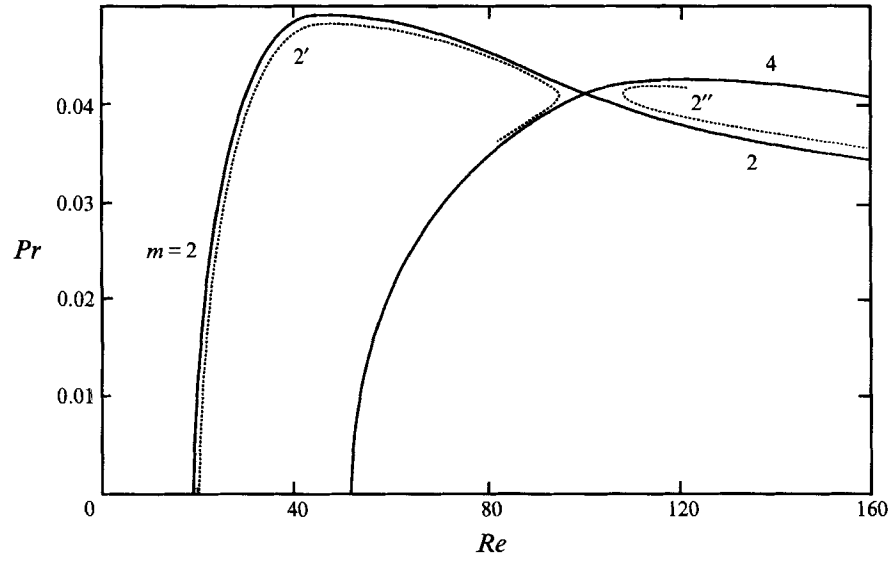

FIGURE 13. Bifurcation and subharmonic resonance at small Pr are illustrated by the arrangement of dashed curves 2′ and 2″ corresponding to the secondary solutions for fixed amplitude and $m = 2$, and neutral curves 2 and 4.

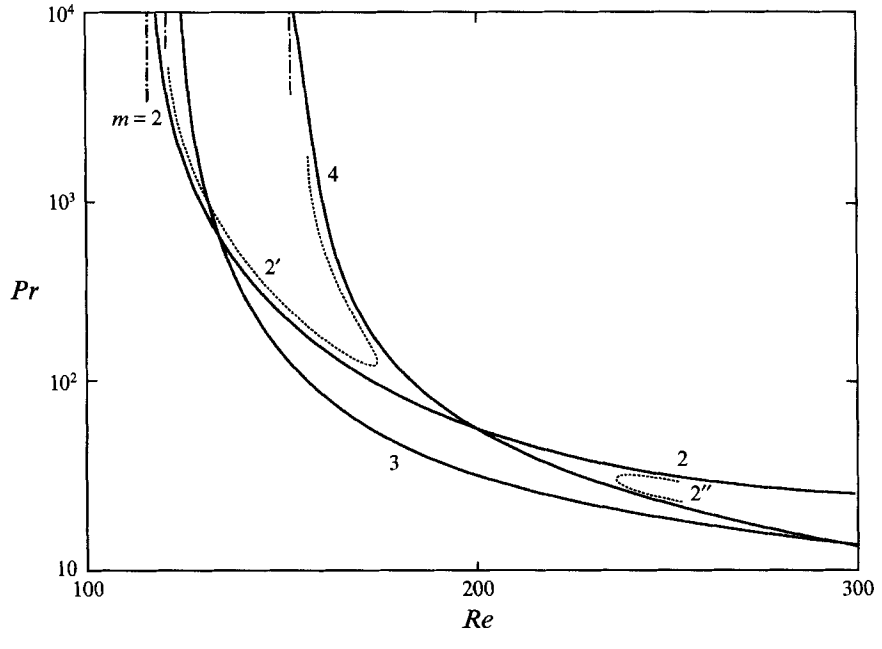

FIGURE 14. The same as figure 13 but for large Pr. The dotted-dashed lines show the limiting values of Re for neutral curves with $m = 1$, 2 and 3.

observed for high Pr (see figure 14). Now, however, the front parts of the neutral curves intersect. This suggests that resonant interactions are possible in experiments where Pr is fixed. Keeping this in mind, we now discuss the behaviour of the secondary solutions and nonlinear subharmonic resonance, observed at a fixed Pr.

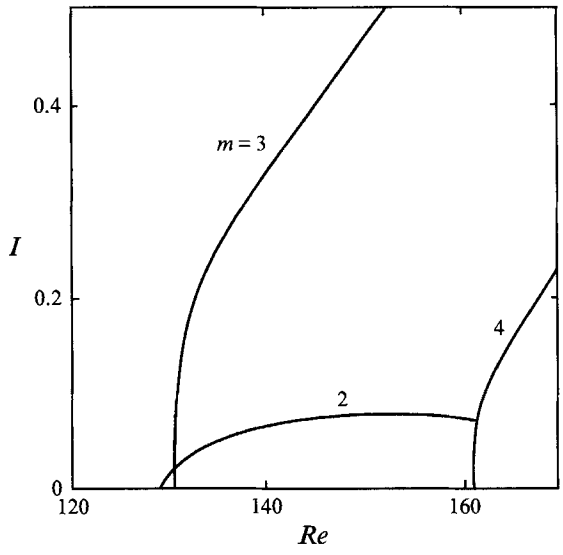

FIGURE 15. Intensity of disturbances for the secondary steady solutions at $Pr = 1000$. The intersection of curves 2 and 4 is related to the secondary bifurcation due to the subharmonic resonance.

10.4. *Secondary solutions at* $Pr = 1000$

As mentioned earlier, the Pr value (actually, the Schmidt number) in the Pshenichnikov & Yatsenko experiment was about 10^3. Figure 15 shows $I(Re)$ for $m = 2$, 3 and 4 at $Pr = 10^3$. Note that the instability is again supercritical. As Re increases, the intensity I for the secondary flow corresponding to $m = 2$ (which bifurcates at $Re = 128.5$) grows rather slowly at first, and then reaches its maximum value $I = 0.08$ at $Re \approx 155$. At the intersection point of curves 2 and 4, the amplitude of the first harmonic in the solution for $m = 2$ becomes zero, and the disturbance energy ($I = 0.073$) is supplied only by the second harmonic. This indicates that a nonlinear subharmonic resonance takes place at the intersection point. Curve 4 corresponds to the secondary solution for $m = 4$ that bifurcates supercritically at $Re = 161.4$, and includes harmonic $\exp(4i\phi)$ and other higher harmonics. However, when the amplitude of the fundamental reaches the critical value, subharmonic bifurcation takes place, and the solution, related to curve 2 in figure 15, branches from the solution for $m = 4$.

An apparent intersection of curves 2 and 3 appears in figure 15 due to projection. This intersection does not indicate additional bifurcation; on the other hand it indicates a possible instability of solution 2 with respect to disturbances corresponding to $m = 3$. Solution 3 at $Re = 130.4$ appears to be unstable with respect to mode $m = 2$ because the basic solution is unstable, and, at the bifurcation points, all the stability characteristics of both the solutions coincide. However, the results shown in figure 15 suggest that, at large amplitudes (i.e. above the intersection point of curves 2 and 3), solution 3 may become stable with respect to the $m = 2$ mode. We may assume that, as Re increases, solution 3 becomes stable while solution 2 loses its stability. This effect would produce a hysteretic transition between regimes of 4 and 6 cells. The experiment by Pshenichnikov & Yatsenko does show such a hysteresis, although the corresponding Re values are 2–3 times more in the experiment (see §4) than in this theory, possibly due to stabilizing effect of the bottom and sidewalls.

11. Discussion

Our analysis reveals that the divergent instability is intimately related to azimuthal symmetry breaking. The divergent instability, which was first found for the planar vortex-source flow (Goldshtik *et al.* 1991), also occurs in three-dimensional fan jets. The study of three-dimensional flows provides a new understanding of the nature of this instability.

The flow divergence (i.e. separation of streamlines with distance from the origin) must be large enough for the divergent instability to occur. It takes place in flows where streamlines of the outflow diverge asymptotically like rays from the origin, but not in the Landau jet and other jet-like flows where the divergence is weaker and the streamlines are asymptotically parabolic.

Two effects related to the influence of boundary conditions are important in the generation of the divergent instability. The first, rather obvious, effect is that of flow stabilization as the surface conditions are changed from slip to no-slip. For the Squire–Wang problem with stress-free conditions for disturbances, we have found $Re_* = 18.9$. However, Re_* becomes 115 for the Marangoni problem at $Pr = \infty$. This increase of Re_* is due solely to the change of the surface conditions from slip to 'half-slip' ones: i.e. the azimuthal velocity becomes zero but the radial velocity does not. When the conditions are no-slip, Re_* becomes infinite. The stabilizing effect of the regularity conditions at the symmetry axis (induced by the smoothing action of viscosity) is similar: when the outflow approaches the axis, Re_* increases to infinity. We have obtained this result for flows in conical regions for cases driven by a boundary force and a body force alike. The second, more complicated, effect of boundary conditions is to increase m_* as the outflow approaches either the no-slip boundary or the axis (see figures 6 and 7). This is, however, quite reasonable, and relates to the localization of short-wave disturbances inside the thin boundary layer (with increasing Re_*) of the outflow – which makes these disturbances less sensitive to outer conditions.

Another intriguing effect is the complete stabilization of the Marangoni convection in the range $0.05 < Pr < 1$. We have studied the energy balance equation and found that the Marangoni stresses provide a sink term in this equation. However, a convincing physical mechanism for the stabilization needs to be found.

The three-dimensional flows investigated here are more stable, as evidenced by higher Re_* values, than the planar flow from the point source examined by Goldshtik *et al.* (1991). Unlike the planar problem, the divergence of streamlines occurs only in a part of the three-dimensional flow region; this provides the above stabilizing effect. Other notable differences are the absence of instability with respect to the disturbance mode $m = 1$ and the supercritical character of bifurcation in the three-dimensional flows. The exact reason for the difference with respect to the mode $m = 1$ is not yet known; our conjecture is that it is related to momentum conservation. If a disturbance of the planar source possesses a non-zero momentum, then it decays asymptotically as $r^{-\frac{1}{3}}$, i.e. more slowly than the basic velocity which decays as r^{-1}. The $m = 1$ mode has non-zero momentum and this results in its relative amplification. Such a reason is absent in the three-dimensional case, where the dependence of the basic flow on r corresponds to the main term of the asymptotic representation. The common feature of all the problems considered here is that no instability occurs with respect to the $m = 1$ mode; thus it prompts us to suggest that the one-jet regime observed by Pshenichnikov & Yatsenko at small Q (figure 3) is not a result of the divergent instability, but is induced by some external source of momentum – which may arise from an asymmetric source.

One more interesting feature of the problem is the intersection of the neutral curves in all the problems considered. The presence of such degeneration in the disturbance spectrum makes possible complex behaviour near the corresponding Re values. In particular, the intersection of the curves corresponding to m and $2m$ corresponds to the subharmonic instability of the secondary solutions. Our results are in qualitative agreement with the experimental observations of Pshenichnikov & Yatsenko regarding both the critical Reynolds number and the patterns of the secondary flows. To obtain better agreement with the experiment, high-amplitude disturbances and their unsteady evolution need to be studied.

12. Summary of results

(i) Bifurcations lead to new steady solutions with azimuthal cells in four problems where a radial divergence of streamlines occurs near a planar or conical surface.

(ii) For the Squire–Wang flow, the minimum $Re_* = 19.2$ corresponds to the azimuthal wavenumber $m = 2$; for $m \gg 1$, the asymptotic law is $Re_* = 2m^2$.

(iii) For the recirculation flow in a conical meniscus, Re_* tends to infinity as the cone angle approaches 0 and π. As the angle decreases, m_* increases.

(iv) A similar instability occurs in two-cell free convection above a rigid cone.

(v) For Marangoni convection in a half-space, two infinite sets of the neutral curves exist which are separated by the interval $0.05 < Pr < 1$. The numerical results for finite Re and Pr, together with the asymptotic solutions for the limiting cases, provide a full analysis of the linear stability problem.

(vi) Nonlinear analysis shows that the primary bifurcations are supercritical and lead to stable secondary regimes. However, secondary subcritical bifurcations and intersections of the neutral curves suggest the presence of regimes with complex dynamics. These results are in accordance with the Pshenichnikov & Yatsenko experiment where both the steady and unsteady regimes are observed.

The authors cordially thank Mikhail Goldshtik and Arindam Ghosh for fruitful discussions and help. This work was supported by Air Force Office of Scientific Research grant F49620-92-J-0200.

Appendix

The system of ordinary differential equations for the nonlinear problem:
for the 'zeroth' harmonic

$$(1-x^2)\,u_0'' = x_y\,u_0' + 2(F_0-u_0) - u_0^2 - \tfrac{1}{2}(y_1\,u_1' + y_2\,u_2' + u_1^2 + u_2^2) - x_m(\Gamma_1\,u_1 + 2\Gamma_2\,u_2);$$

$$(1-x^2)\,F_0' = x_m(\Gamma_1\,y_1 + 2\Gamma_2\,y_2) - \tfrac{1}{2}(\Gamma_1\,\Gamma_1' + \Gamma_2\,\Gamma_2');$$

$$y_0' = u_0; \quad x_y = x_2 - y_0; \quad x_m = m/[2(1-x^2)]; \quad x_2 = 2x;$$

$$(1-x^2)\,\vartheta_0'' = x_2\,\vartheta_0' - Pr[y_0\,\vartheta_0' + u_0\,\vartheta_0 + \tfrac{1}{2}(y_1\,\vartheta_1' + y_2\,\vartheta_2' + u_1\,\vartheta_1 + u_2\,\vartheta_2) + x_m(\Gamma_1\,\vartheta_1 + 2\Gamma_2\,\vartheta_2)];$$

for the first harmonic

$$(1-x^2)\,u_1'' = x_2\,u_1' + 2(F_1-u_1) + x_{m2}\,u_1 - [y_1(u_0' + \tfrac{1}{2}u_2') + u_1'\,y_{02} + 2u_{02}\,u_1 + x_m(\Gamma_2\,u_1 + 2\Gamma_1\,u_2)];$$

$$(1-x^2)\,\Gamma_1'' = m(F_1+u_1)+x_{m2}\,\Gamma_1-y_0\,\Gamma_1'-\tfrac{1}{2}(y_1\,\Gamma_2'-y_2\,\Gamma_1')+x_m\,y_1(2x_x+y_2);$$

$$(1-x^2)\,F_1' = m\Gamma_1'-x_{m2}\,y_1-\tfrac{1}{2}(\Gamma_1\,\Gamma_2'+\Gamma_2\,\Gamma_1')+x_m(\Gamma_2\,y_1+2\Gamma_1\,y_2);$$

$$y_1' = u_1+2x_m\,\Gamma_1;\quad x_{m2}=m^2/(1-x^2);\quad u_{02}=u_0+\tfrac{1}{2}u_2;\quad y_{02}=y_0+\tfrac{1}{2}y_2;$$

$$(1-x^2)\,\vartheta_1'' = x_2\,\vartheta_1'+x_{m2}\,\vartheta_1-Pr[y_1(\vartheta_0'+\tfrac{1}{2}\vartheta_2')+\vartheta_1'\,y_{02}+u_1(\vartheta_0+\tfrac{1}{2}\vartheta_2)$$
$$+\vartheta_1\,u_{02}+x_m(\Gamma_2\,\vartheta_1+2\Gamma_1\,\vartheta_2)];$$

for the second harmonic

$$(1-x^2)\,u_2'' = x_y\,u_2'+2(F_2-u_2-u_0\,u_2)+x_{m4}\,u_2-y_2\,u_0'-\tfrac{1}{2}(y_1\,u_1'+u_1^2)+x_m\,\Gamma_1\,u_1;$$

$$(1-x^2)\,\Gamma_2'' = 2m(F_2+u_2)+x_{m4}\,\Gamma_2-(y_0\,\Gamma_2'+\tfrac{1}{2}y_1\,\Gamma_1')+x_m(4x_x\,y_2+y_1^2);$$

$$(1-x^2)\,F_2' = 2m\Gamma_2'-x_{m4}\,y_2+\Gamma_1(\tfrac{1}{2}\Gamma_1'-x_m\,y_1);$$

$$y_2' = u_2+4x_m\,\Gamma_2;\quad x_{m4}=4x_{m2};\quad x_x=x_2+y_0;$$

$$(1-x^2)\,\vartheta_2'' = x_2\,\vartheta_2'+x_{m4}\,\vartheta_2-Pr[y_0\,\vartheta_2'+\vartheta_0'\,y_2+u_0\,\vartheta_2+u_2\,\vartheta_0-x_m\,\Gamma_1\,\vartheta_1+\tfrac{1}{2}(y_1\,\vartheta_1'+u_1\,\vartheta_1)];$$

REFERENCES

BAYLEY, A. G. 1988 *Electrostatic Spraying of Liquids*. Wiley.

BRATUKHIN, YU. K. & MAURIN, L. M. 1967 Thermocapillary convection in a fluid filling a half-space. *J. Appl. Math. Mech.* **31**, 605–608.

GOLDSHTIK, M. A., HUSSAIN, F. & SHTERN, V. N. 1991 Symmetry breaking in vortex-source and Jeffery-Hamel flows. *J. Fluid Mech.* **232**, 521–566.

GOLDSHTIK, M. A. & SHTERN, V. N. 1990*a* Collapse in conical viscous flows. *J. Fluid Mech.* **218**, 483–508.

GOLDSHTIK, M. A. & SHTERN, V. N. 1990*b* Free convection near a thermal quadrupole. *Intl J. Heat Mass Transfer* **33**, 1475–1483.

GUCKENHEIMER, J. & HOLMES, P. J. 1983 *Nonlinear Oscillations, Dynamical Systems, and Bifurcations of Vector Fields*. Springer.

HAYATI, I., BAYLEY, A. I. & TADROS, TH. F. 1986 Mechanism of stable jet formation in electrohydrodynamic atomization. *Nature* **319**, 41–43.

JOSEPH, D. D. 1976 *Stability of Fluid Motions, Vol. 1*. Springer.

LEVICH, V. G. 1962 *Physicochemical Hydrodynamics*. Prentice Hall.

PSHENICHNIKOV, A. F. & YATSENKO, S. S. 1974 Convective diffusion from localized source of surfactant. *Hydrodynamics* V, 175–181 (*Scientific papers of Perm University*, in Russian).

SQUIRE, B. 1952 Some viscous fluid flow problems. 1. Jet emerging from a hole in a plane wall. *Phil. Mag.* **43**, 942–945.

WANG, C. V. 1971 Effect of spreading of material of the surface of a liquid. *Intl J. Nonlinear Mech.* **6**, 255–262.

WANG, C. V. 1991 Exact solutions of the steady-state Navier–Stokes equations. *Ann. Rev. Fluid Mech.* **23**, 159–177.

YUDOVICH, V. I. 1965 Stability of steady flows of viscous incompressible fluid. *Sov. Phys. Dokl.* **10**(4), 293–295.